Real-time observation of the coherent transition to a metastable emergent state in $1T$-TaS_2

Jan Ravnik,[1] Igor Vaskivskyi,[1,2] Tomaz Mertelj,[1,2] and Dragan Mihailovic[1,2]
[1]*Jozef Stefan Institute, Jamova 39, SI-1000 Ljubljana, Slovenia*
[2]*CENN Nanocenter, Jamova 39, SI-1000 Ljubljana, Slovenia*

(Received 4 October 2017; revised manuscript received 12 January 2018; published 12 February 2018)

The transition to a hidden metastable state in $1T$-TaS_2 is investigated in real time using coherent time-resolved femtosecond spectroscopy. Relying on spectral differences between phonon modes in the equilibrium states and in the metastable state, and temperature-tuning the metastable state lifetime, we perform stroboscopic measurements of the electronic response and switching of coherent oscillation frequency through the transition. Very fast coherent switching of the collective-mode frequency is observed (∼400 fs), comparable to the electronic time scale ∼300 fs. A slower, 4.7-ps process is attributed to lattice relaxation. The observations are described well by a fast electronic band structure transformation into the metastable state, consistent with a topological transition.

DOI: 10.1103/PhysRevB.97.075304

I. INTRODUCTION

Metastable many-body states are manifestations of collective effects which are of great importance in different areas of science, from the false vacuum state in field theory of elementary particles to potential uses in memory devices. The microscopic mechanisms leading to such metastable states, and particularly the transition dynamics, are still relatively unexplored. In condensed matter systems exhibiting electronic order, a transient particle-hole imbalance may lead to the creation of transient emergent states, whose structure may be different than any equilibrium states, as illustrated by a recent example of photoexcited "hidden" (H) state in the layered dichalcogenide $1T$-TaS_2 [1–3] [Fig. 1(a)]. This material is an extremely versatile model system which has experienced a recent resurgence of interest because it exhibits a number of equilibrium and nonequilibrium phases [1,3] [Fig. 1(b)] where conventional ordering mechanisms do not apply. Competing Fermi surface instabilities, strain, and Coulomb repulsion in combination with out-of-plane "orbitronics" [4] lead to a multidimensional phase diagram which includes a Mott insulator phase, a metallic phase, and a superconducting phase. A quantum spin liquid–like state was reported below 220 K, adding to its complexity [5]. One of the consequences of competing interactions is that there is a sequence of charge-density wave (CDW) transitions starting with a transition from a metallic state above 550 K to an incommensurate (IC) CDW state, followed at $T_{c2} = 350$ K by an unusual strain-driven transition [6] exhibiting a partial Kohn anomaly [7–9] to a "nearly commensurate" (NC) state composed of domain walls (discommensurations) and commensurate domains. This unusual transition, whose topological nature was discussed already by McMillan [7] is of great recent interest, as it is believed to play a role in metastable state formation [1,10]. Eventually the discommensurations disappear below $T_{c3} \simeq 180$ K in the transition to an insulating commensurate (C) charge-ordered state. On heating from the C state, transition to the trigonal (T) phase takes place at $T_{C-T} = 220$ K, which survives up to 280 K. We are concerned here with the mechanism for the transition between the insulating C state and a metallic metastable hidden (H) state which takes place under nonequilibrium conditions. Initial experiments showed that short optical pulses may trigger such a transformation, but there is so far little indication on what time scale the new state settles into long-range order. The fundamental issue is whether the transition takes place diffusively or coherently. In the diffusive case, carriers from the C ground state are delocalized by the short, 30-fs pulse whereupon they first localize in pseudorandom positions, and later form the textured domain structure [2] through a combination of diffusive electron motion [11] and incoherent atomic ordering [1], followed by domain wall nucleation and growth on a 300–400-ps time scale as observed by x-ray diffraction at the NC-IC transition [12]. Alternatively, in a coherent transition, the transition to a long-range ordered metastable state takes place on an electronic time scale, starting with a many-body interference of nested nonequilibrium Fermi surface electrons followed by an adjustment to the lattice. In this case, the lattice is expected to adapt rapidly to the new electronic order forming a new periodic lattice distortion without any intermediate diffusive processes. Secondary relaxation of strain between the incommensurate electronic order and the underlying crystal lattice would then follow on much longer time scales. Another important question is what is the difference between the H state and a supercooled NC state [13], which is also related to the fundamental mechanism of formation of the H state.

The problem with investigating long-lived metastable states created by photoexcitation is that the transition is caused by a singular event—such as a single-shot laser pulse. The state of the system before and after the transition can be investigated in detail by equilibrium techniques [1,2], but not the dynamics of the event itself. The H metastable state lifetime in $1T$-TaS_2 has recently been discovered to be tunable by a combination of substrate strain and temperature [14,15], so provided the system can be made to relax in between laser pulses, stroboscopic pump-probe measurements of the collective- and single-particle dynamics *through* the C-H transition can be performed. While at 4 K the extrapolated H state lifetime is $>10^{18}$ s, at 160 K the lifetime is $\tau_H < 10^{-4}$ s, and the relaxation of the photoinduced state is sufficiently fast to allow measurements

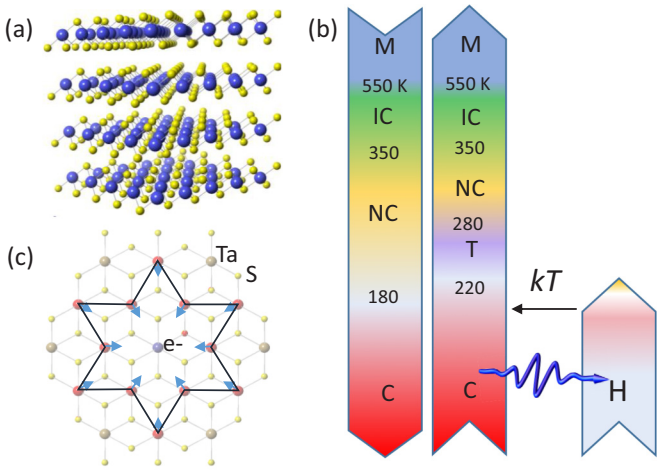

FIG. 1. (a) The structure of $1T$-TaS_2. (b) Schematic phase diagram of $1T$-TaS_2 upon cooling, warming, and after photoexcitation. (c) A schematic diagram of the atomic displacements corresponding to the dominant breathing "amplitude mode" in the C state.

with a 1-kHz repetition rate laser. At this base temperature, photoexcitation with pulse fluences of $\sim$1 mJ/cm^2 leads to heating of both the electrons and the lattice well above $T_{C-T} =$ 220 K, so we might expect that either the H state, the NC or T state, or possibly some other nonequilibrium state might form [3]. Distinguishing the ordering vectors [2] between the H and NC states requires currently unavailable resolution with time-resolved electron diffraction or x-ray techniques [12,16], so the ordering dynamics cannot be measured directly by diffraction techniques. One possibility to discern between coherent and incoherent domain wall dynamics would be to investigate the linewidth of the mode commonly assigned to the amplitude mode (AM) [whose displacements are shown in Fig. 1(c)], similarly as was previously used to measure the coherent evolution of the order parameter through the CDW transition in $TbTe_3$ [17]. Alternatively, here we show that one can measure the apparent shift of the AM frequency associated with the transition [1] in real time using coherent phonon spectroscopy with multiple laser pulses.

II. EXPERIMENT

We prepare a single crystal of $1T$-TaS_2 using a previously reported method [1]. The size of the crystal is 2 × 2 × 0.3 mm^3. The sample is held in a cryostat and cooled down with liquid nitrogen to 160 K. The cooling is done at a rate of 1 K/min to prevent supercooling of high-temperature states.

The spectra are measured with two-pulse pump-probe and three-pulse destruction-pump-probe spectroscopy and are individually described later. We use a Ti:sapphire laser at 800 nm with a pulse length of 30 fs and a repetition rate of 1 kHz. The beam spots on the sample are between 30 and 50 μm in diameter with the destruction beam spot being the biggest and the probe beam spot the smallest, to prevent the measurements of unmodulated areas of the sample. In the experiment, the pump beam is chopped by a mechanical chopper with half of the laser frequency (500 Hz) to let every second pump pulse through. We measure the probe beam in reflection configuration with balanced diode detection using a lock-in amplifier. The destruction pulse, when used, is not chopped and not monitored. The fluences of pump and probe pulses are kept low at 0.2 and 0.05 mJ/cm^2, respectively, to minimally disturb the sample, while the fluence of the destruction pulse is much higher, to induce observable changes.

III. RESULTS

We first need to determine if the H state can be unambiguously distinguished from other states by its phonon spectrum, and particularly from the supercooled NC state which has been reported in thin flakes [10]. In Fig. 2(a) we show the coherent reflectivity oscillations of $1T$-TaS_2 obtained at different temperatures. The C and H states are measured with three-pulse destruction-pump-probe spectroscopy, where the destruction (D) pulse arrives 50 ps and 1 ms before the pump-probe sequence to measure the H and relaxed C states, respectively. Measurements of the NC and T states were done with a standard two-pulse pump-probe technique. Fourier transformed phonon spectra together with fits to three sets of coherent oscillations by the displacive excitation mechanism using Eq. (1) from [18]) are shown in Fig. 2(b). We see that the spectra in the four phases differ substantially. A summary of the T dependences of our observed phonon peak positions in different (equilibrium) phases is shown in Fig. 2(c), including Raman data (the Brillouin-zone center phonons $q \simeq 0$) [19]. To show the origin of the soft modes, we also include neutron [20] and x-ray frequencies at the wave vector of the observed Kohn anomaly ($q = 0.26$ reciprocal lattice units) [9] at the IC-NC transition. In the C state, the low-frequency spectrum below 4 THz (120 cm^{-1}) consists of Ta modes derived from folding of high-temperature acoustic modes into the commensurate Brillouin zone [19]. Above 220 K, in the IC and NC states, modes appear in the Raman spectra whose origin can be traced to the Kohn anomaly near the NC-IC transition seen in the x-ray and neutron data, and a number of soft modes associated with the transition can be identified at low temperatures [19]. A softened longitudinal acoustic (LA) mode associated with the observed Kohn anomaly at $q = 0.28$ r.l.u. along the crystal axes modulates the parent $1T$ structure to give the IC phase [9]. An accompanying softened transverse acoustic $TA_{||}$ mode induces the rotation of the overall ordering vector to accommodate the ordering of commensurate domains and discommensurations in the NC state. The NC structure, and similarly the H structure [2], can be described in terms of a superposition of different wave vectors (harmonics). Phonons whose wave vectors correspond to these harmonics may partially condense or soften in different points of the Brillouin zone, giving multiple collective modes in the folded Brillouin zone [19,21]. In the C phase, as the discommensurations disappear, the collective "amplitude" mode becomes dominant in the spectrum [Fig. 1(c)]. The intensity of the coherent oscillation (and Raman) spectra reflects the mode coupling to the electronic modulation, and the photon resonances for displacive excitation and detection as described by the stimulated Raman tensor [22]. The resonances depend on the electronic structure in the vicinity of the Fermi level, and are particularly sensitive to orbital ordering and change of symmetry [23]. This can be easily understood if we write the Raman tensor in terms of the derivative of the

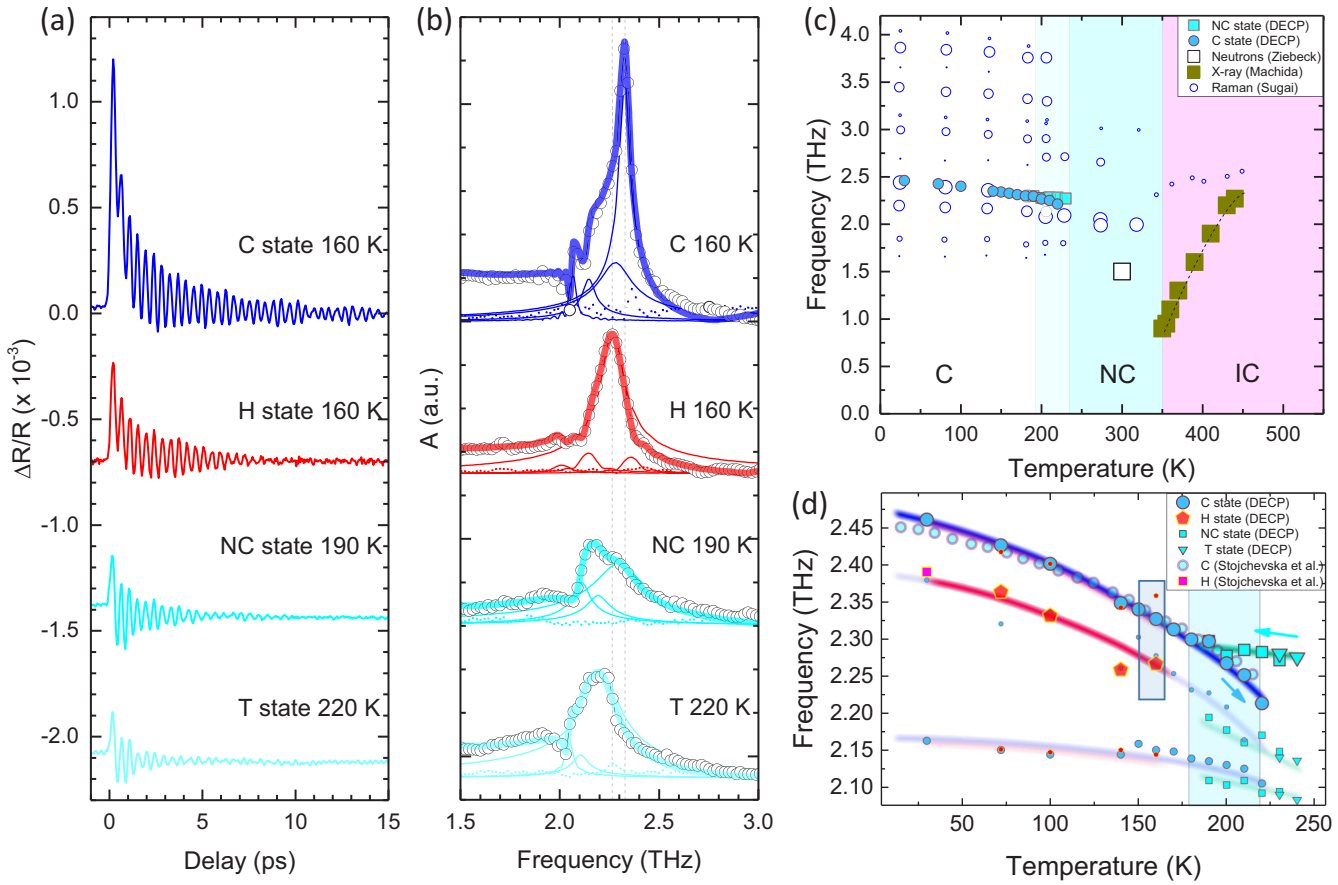

FIG. 2. (a) Time-resolved reflectivity of $1T$-TaS_2 in different states, which show exponential quasiparticle decay with superimposed oscillatory response from coherent excitation of collective modes and (b) their fast Fourier transforms. Dots are the experimental data; thick lines are fits with the DECP model [18]. Thin lines are individual oscillators used for the DECP fit, with only the oscillatory part plotted. The transition from the C to the H state results in a shift of intensity to a lower frequency (dashed vertical lines). In the NC and T states, peaks at even lower frequencies appear and become more prominent with higher temperature. (c) Temperature dependence of the collective-mode frequencies combined from different techniques [9,19,20] shown in the legend. (d) Temperature dependence of the mode frequencies. The size of the symbols and color intensity of the streaks represent the intensity of the corresponding modes in the C, H, NC, and T phases in blue, red, cyan, and light cyan, respectively.

complex dielectric constant $\boldsymbol{\varepsilon}(\omega)$ with respect to the phonon displacement Q : $\boldsymbol{R}(\omega) = d\boldsymbol{\varepsilon}(\omega)/dQ$, where $\boldsymbol{\varepsilon}(\omega)$ depends on the joint density of electronic states involving optical transitions between states near E_F and 1.5 eV above or below it [24].

Here we shall focus on the spectral differences obtained by pump-probe spectroscopy in the vicinity of the AM [19] at 2.3 THz in the C, H, and NC states [Fig. 2(d)]. For the H state measurements, an initial switching pulse preceding the pump-probe pulses of a few hundred picoseconds was used to transiently drive the system into the H state. Comparing the spectra near the AM frequency in equilibrium phases with the H phase, we see quite remarkable differences [Figs. 2(b) and 2(d)]. Three modes (at ω_1, ω_2, and ω_3) are observed in all four phases [Fig. 2(b)]. However, their intensities are drastically different, and each phase has a unique spectral fingerprint. The differences between the H and NC spectra are particularly remarkable. The origin of the spectral differences may be attributed to the high sensitivity of the low-energy band structure to orbital order [4], so differences in the long-range domain order may also result in different resonant coherent phonon intensities.

In addition to in-plane domain ordering, calculations by Ritschel *et al.* [4] showed that different stacking of the charge-density wave along the c axis can lead to either metallic or insulating phases, depending on the Ta $5d$ "orbital textures". Band structure calculations show that the stacking appears to have a very strong effect not only on out-of-plane electronic bands, but also on in-plane bands near E_F. Since the AM displacements predominantly involve Ta atoms [Fig. 1(c)], the electron-phonon coupling is strongly dependent on the Ta $5d$ orbital texture. This can lead to further phonon mode differences in frequency and intensity between the H, C, and NC phases.

Having established that the AM frequency can be used as a fingerprint of the H state, we perform a stroboscopic three-pulse experiment at 160 K, where the metastable H-state lifetime ($<100\,\mu$s) is much shorter than the time between pulses (1 ms) [14]. To determine the real-time trajectory through the C-H transition on short time scales first, a chopped beam of pump (P) pulses is applied starting a coherent oscillation of the collective modes, which are recorded by reflectivity oscillations $\Delta R(t)$, recorded by a lock-in amplifier

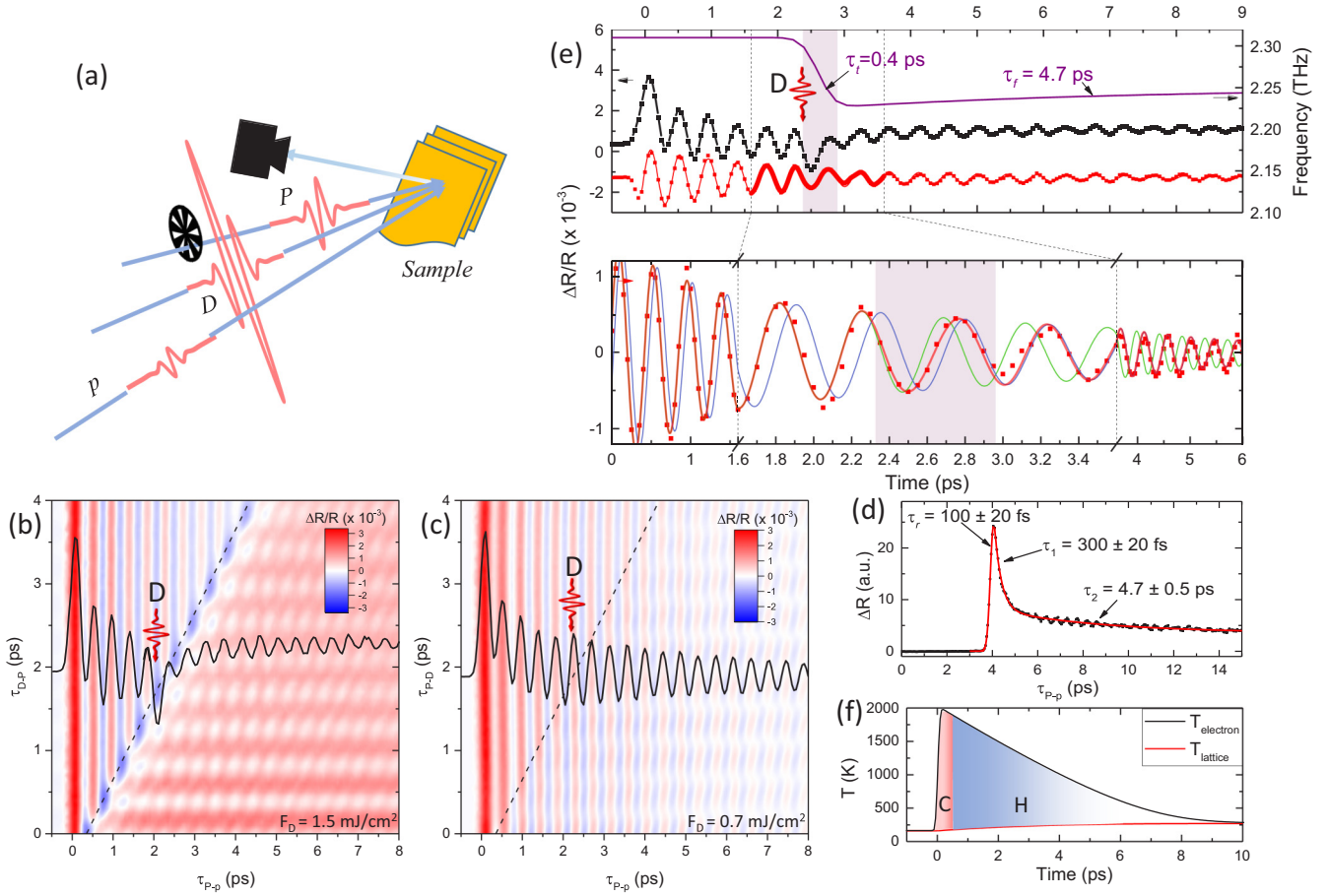

FIG. 3. (a) Schematic diagram of the optical three-pulse experiment. (b,c) Three-pulse P-D-Pr traces for D pulse fluence adjusted above ($F_D = 1.5\,\mathrm{mJ/cm^2}$) and below ($F_D = 0.7\,\mathrm{mJ/cm^2}$) switching threshold, respectively. Dashed line shows the time of the D pulse arrival. Black curve is a single trace for selected τ_{P-D}. (d) Standard two-pulse pump-probe trace with above-threshold pump pulses ($F_P = 1.5\,\mathrm{mJ/cm^2}$). The reflectivity of the sample possesses fast rise and double-exponent relaxation. (e) Detailed analysis of the P-D-Pr trace for $\tau_{P-D} = 2.6$ ps (black) and extracted oscillatory response only (red dots) with FM sine fit (red line). The frequency profile used for the fit is shown in purple. Bottom panel: the same data zoomed in around $\tau_{P-p} = \tau_{P-D}$. Dashed lines are sine fits before (blue) and after (green) the D pulse arrival using constant frequency ω_C and ω_H, respectively. The narrow region, in which the phase shift occurs and both fits diverge from data, is highlighted. (f) Estimation of electron and lattice temperature after the D pulse arrival using a two-temperature model for $F_D = 1.5\,\mathrm{mJ/cm^2}$ [1].

and a variably time-delayed probe (p) pulse. [A schematic diagram of the experiment is shown in Fig. 3(a).] The H state transition is induced at variable delays after the P pulse by the D pulse. Fluence of the D pulse is adjusted above and below the switching threshold (∼1 mJ/cm^2) while the P and p fluences are kept constant. The direct change of the reflectivity, ΔR_D, due to the D-pulse-induced transition and the change in the frequency of the P-pulse-induced coherent oscillations induced by the transition are recorded. The results are shown in Figs. 3(b) and 3(c) above and below the switching threshold [1] as a function of time delay τ_{P-D} between the P and D pulses. The fluences of the D pulse were set above and below the switching threshold at 1.5 and 0.7 mJ/cm^2, respectively. The transition caused by the D pulse is clearly observed from the change of the coherent oscillation pattern. To analyze the change quantitatively we make an expanded plot at one τ_{P-D} delay [shown superimposed on the two-dimensional plot in Fig. 3(b)] and focus only on the oscillatory signal by subtracting exponentially decaying components of the transient reflectivity [Fig. 3(e)]. We clearly see a frequency change in the magnified plot of the coherent oscillations which takes place in a time interval between $\tau_{P-p} = 2.4$ ps and 2.8 ps on the time axis. Fitting the oscillations with a function of the form $\sim \sin[\omega(t)t]$ reveals a steplike change of the collective-mode frequency from 2.31 to 2.23 THz within $\tau_t \sim 400$ fs [top trace, Fig. 3(e)], followed by a small frequency shift on a time scale of 4.7 ± 1 ps reaching the long-time value of $\omega_H = 2.25$ THz. The frequency transition time τ_t corresponds approximately to one mode oscillation period ($T^C_{AM} = 0.44$ ps). Below the switching threshold [Fig. 3(c)] ($F_D = 0.7\,\mathrm{mJ/cm^2}$), no transition is observed, and as expected, there is no measurable change of the frequency since the initial and final states are the same.

The C-H transition is accompanied by an increase of reflectivity of $\Delta R_D \sim 5\%$ at 800 nm with a rise time $\tau_r \lesssim 100$ fs, consistent with observed melting of the C state [25]. Thereafter, the reflectivity relaxes with two characteristic lifetimes ($\tau_1 \simeq 300 \pm 20$ fs and $\tau_2 \simeq 4.7 \pm 0.5$ ps). The two transients of the frequency and reflectivity switching, given by $\tau_t = 400$ fs and $\tau_e = 300$ fs, respectively, characterize the initial transition

followed by processes on a time scale of ∼ 4.7 ps, previously attributed to the lattice relaxation at the IC-NC transition [26].

IV. DISCUSSION AND MODELING

To understand the observed behavior of the coherent AM oscillation through the C-H transition, and the meaning of the observed lifetimes, we need to consider the sequence of ordering events leading to the eventual creation of the H state. In equilibrium, at high temperatures, the single-band metallic system [27] is susceptible to a transition to an incommensurate state driven by Fermi surface (FS) nesting which occurs at 550 K [28]. In the photoexcited state, however, experimentally $1T$-TaS_2 shows a significant e-h asymmetry [29], indicating a shift of the chemical potential (photodoping) and a warped photoexcited FS. On the time scale of 300 ∼ 400 fs where the transition takes place, the estimated effective electronic temperature given by the two-temperature model is possibly >1000 K [1,29] [the estimated temperatures are shown in Fig. 3(f)]. While we should not take this temperature to be very accurate, the implication is that the ordering of nested FS electrons takes place outside of equilibrium. At the end of this process, we can conclude that the resulting transient CDW state will have a modulation wave vector which is different from the equilibrium one. The next step is the mutual adjustment of the nonequilibrium electronic order and the lattice. The observed $\tau_2 \sim 4.7$ ps [Fig. 3(d)] is consistent with the time for the formation of a periodic lattice distortion in the NC state measured by ultrafast electron diffraction [26,30]. It is also consistent with the thermalization time τ_{th} of the electrons with the lattice given by the two-temperature model ($\tau_{th} = 4 \sim 5$ ps) shown in Fig. 3(f). τ_2 is also consistent with the anharmonic lifetime $\tau_{anh} \sim 5.9$ ps given by the Lorentzian linewidth of the AM in the H state (0.17 THz) which signifies the time needed for energy of the AM to be released to other coupled lattice modes. After this time, the accommodation of remaining strain due the incommensurability between the transient electronic order and the lattice leads to the formation of commensurate

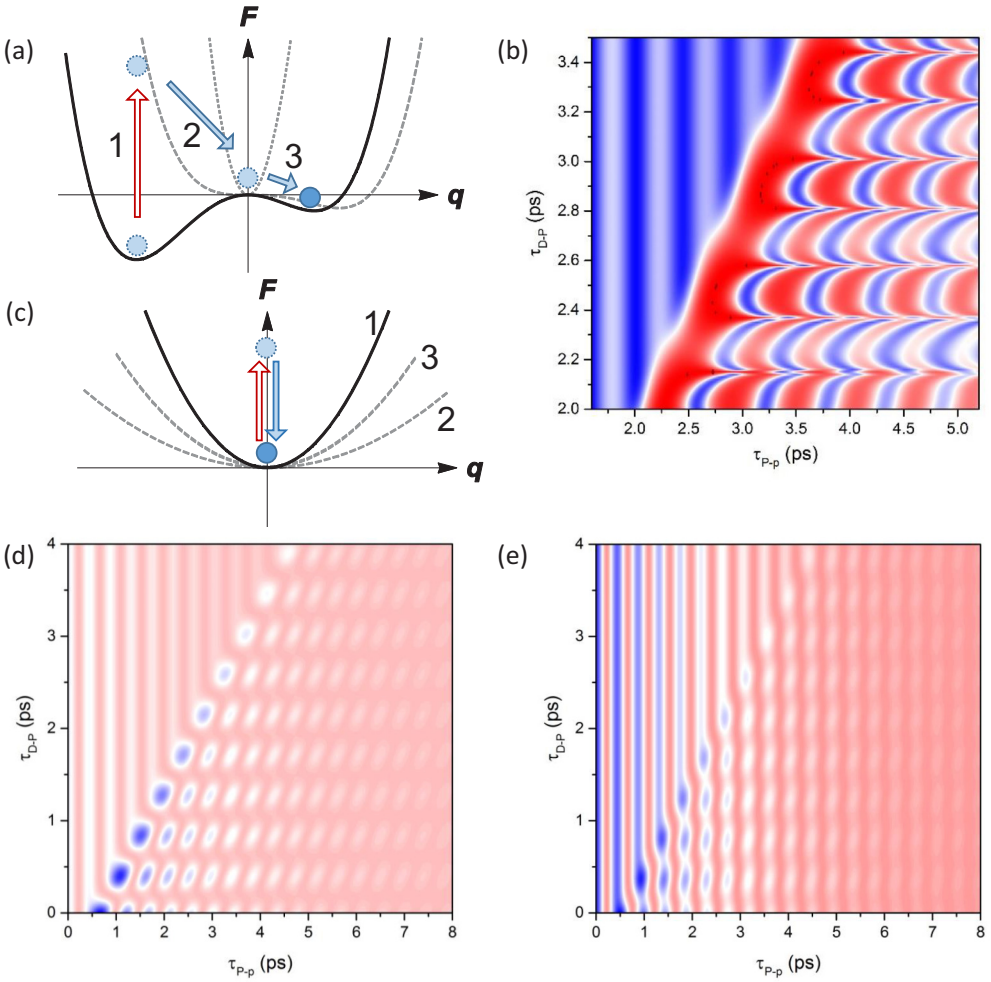

FIG. 4. (a) Time evolution of anharmonic potential used for simulations with Ginzburg-Landau theory. Starting from global minimum on free-energy surface (1) the D pulse drives the system to the high-symmetry state (2), from which it thermalizes via intermediate states (3) to the new metastable state, which corresponds to the local minimum on the equilibrium free-energy surface (4). (b) Simulated three-pulse spectrum using a Ginzburg-Landau model (a). (c) Evolution of quadratic potential used for the topological model. Starting from the ground state (1), the system follows to the transient state with high concentration of discommensurations (2), which then decrease to the new, nonzero value (3) [1]. (d,e) Results of simulations with model from (c) for F_D above and below the switching threshold, respectively.

domains and discommensurations in the new metastable H state.

To model the transition quantitatively, we first attempt to use a model based on a time-dependent Ginzburg-Landau theory for a first-order transition with a time-dependent potential to describe the metastable state shown schematically in Fig. 4(a). The time scale for the formation of the metastable state indicated by experiments is the electronic τ_1, followed by lattice ordering on a time scale of τ_2. The metastable state naturally arises through a third-order term in the free-energy expansion $F = a(t)\psi^2 - b(t)\psi^3 + c\psi^4$, as allowed by symmetry of the triple CDW in $1T$-TaS_2 [31], where ψ corresponds to the dimensonless order parameter. The time dependence in the potential [32] can then be introduced through experimental decay constants in the form $a(t) = a_0[1 - \exp(-t/\tau_1)]$, $b(t) = b_0[1 - \exp(-t/\tau_2)]$. c is a positive constant to ensure the overall stability of the model. Numerical simulations of the transient reflectivity based on equations of motion derived from this model, under the assumption that the transient reflectivity is proportional to the order parameter $\Delta R \sim \Delta(\psi^2)$ [32], are shown in Fig. 4(b). Even with significant adjustment of the parameters, agreement with the experimental data in Fig. 3(b) is hardly satisfactory, showing that modeling in terms of an order parameter trajectory through an ordering transition that was used successfully to describe $TbTe_3$ [32] does not work here.

Following the notion that the transition cannot be described using Landau theory with a conventional order parameter, we consider the effect of the change of electronic structure of states near E_F associated with the insulator-metal topological transition on the collective-mode spectrum. To describe the frequency shift phenomenologically (which includes the effect of a resonant crossover between ω_2 and ω_3), we can write $\omega = \omega_C - \delta(t)$. We can then calculate the transient reflectivity dynamics of the AM through the transition using a simple quadratic potential $F = \frac{\omega^2(t)}{2}\psi^2$ with an equation of motion $\frac{1}{\omega^2}\psi'' + \frac{\alpha}{\omega}\psi' + \psi = 0$, where to first order $\omega^2(t) = \omega_C^2 - 2\omega_C\delta(t)$, and $\delta(t) = \frac{1}{2}[\eta_1 + \eta_2 e^{-t/\tau_1} + \eta_3 e^{-t/\tau_2}][1 + \mathrm{erf}(\frac{t}{\tau_r})]$. The parameter α describes the damping and was set to fit the experimental values. The predicted transient reflectivity response within this model is very sensitive to the fast time evolution of the overall frequency trajectory. In Fig. 4(d) we show the predicted behavior with an electronic time scale transition to the metastable state: $\tau_1 = 300$ fs only ($\eta_3 = 0$) with a finite long-delay frequency shift η_1. For comparison, the reflectivity for $\eta_1 = 0$ is shown in Fig. 4(e). We see that in both cases the model compares well with the observed transient reflectivity data in Figs. 3(b) and 3(c), above ($\eta_1 > 0$) and below ($\eta_1 = 0$) the switching threshold. Adding the third term ($\eta_3 \neq 0$) with $\tau_2 = 4.7$ ps in $\delta(t)$ gives a barely perceptible change in the predicted response, from which we conclude that the change of ω is predominantly the result of electronic ordering into the H state, while the lattice response which occurs on a time scale of τ_2 has little effect on the AM. τ_r is the rise time, which was measured to be 100 fs.

V. CONCLUSIONS

The use of coherent mode dynamics through the transition highlights the electronic nature of the transition driving the ordering in the H state on a time scale <400 fs. We conclude that the C-H transition cannot be described in terms of a time evolution of a Landau order parameter through a first-order transition. Rather, it is consistent with a nonequilibrium topological transition from a uniform state to a textured state with an accompanying change of electronic structure giving rise to good agreement with the phonon mode dynamics through the transition. The marked difference in the H and NC state mode spectra is quite surprising, implying that their electronic structure near the Fermi level is substantially different, in spite of the fact that both are composed of long-range order of commensurate domains and discommensurations which look qualitatively similar in scanning tunneling microscopy [2]. Understanding the origin of the difference in electronic structure of different states and in particular between H and NC states will be important for establishing the microscopic mechanism promoting metastability of the transient emergent state.

ACKNOWLEDGMENTS

We acknowledge discussions and comments from S. Brazovskii. The authors would like to acknowledge the financial support from Slovenian Research Agency (ARRS), project P1-0040, ERC ADG GA Grant No. 320602 Trajectory.

[1] L. Stojchevska, I. Vaskivskyi, T. Mertelj, P. Kusar, D. Svetin, S. Brazovskii, and D. Mihailovic, Science **344**, 177 (2014).
[2] Y. A. Gerasimenko, I. Vaskivskyi, and D. Mihailović, arXiv:1704.08149v2 [cond-mat.str-el].
[3] T.-R. T. Han, F. Zhou, C. D. Malliakas, P. M. Duxbury, S. D. Mahanti, M. G. Kanatzidis, and C.-Y. Ruan, Science **1**, e1400173 (2015).
[4] T. Ritschel, J. Trinckauf, K. Koepernik, B. Büchner, M. von Zimmermann, H. Berger, Y. I. Joe, P. Abbamonte, and J. Geck, Nat. Phys. **11**, 328 (2015).
[5] M. Klanjšek, A. Zorko, R. Žitko, J. Mravlje, Z. Jaglicic, P. K. Biswas, P. Prelovšek, D. Mihailovic, and D. Arčon, Nat. Phys. **13**, 1130 (2017).
[6] F. Clerc, C. Battaglia, M. Bovet, L. Despont, C. Monney, H. Cercellier, M. G. Garnier, P. Aebi, H. Berger, and L. Forro, Phys. Rev. B **74**, 155114 (2006).
[7] W. McMillan, Phys. Rev. B **14**, 1496 (1976).
[8] K. Nakanishi and H. Shiba, J. Phys. Soc. Jpn. **45**, 1147 (1978).
[9] Y. Machida, T. Hanashima, K. Ohkubo, K. Yamawaki, M. Tanaka, and S. Sasaki, J. Phys. Soc. Jpn. **73**, 3064 (2004).
[10] M. Yoshida, R. Suzuki, Y. Zhang, M. Nakano, and Y. Iwasa, Sci. Adv. **1**, e1500606 (2015).
[11] D. F. Shao, R. C. Xiao, W. J. Lu, H. Y. Lv, J. Y. Li, X. B. Zhu, and Y. P. Sun, Phys. Rev. B **94**, 125126 (2016).
[12] C. Laulhé, T. Huber, G. Lantz, A. Ferrer, S. O. Mariager, S. Grübel, J. Rittmann, J. A. Johnson, V. Esposito, A. Lübcke,

L. Huber, M. Kubli, M. Savoini, V. L. R. Jacques, L. Cario, B. Corraze, E. Janod, G. Ingold, P. Beaud, S. L. Johnson *et al.*, Phys. Rev. Lett. **118**, 247401 (2017).

[13] M. Yoshida, Y. Zhang, J. Ye, R. Suzuki, Y. Imai, S. Kimura, A. Fujiwara, and Y. Iwasa, Sci. Rep. **4**, 7302 (2014).

[14] I. Vaskivskyi, J. Gospodaric, S. Brazovskii, D. Svetin, P. Sutar, E. Goreshnik, I. A. Mihailovic, T. Mertelj, and D. Mihailovic, Sci. Adv. **1**, e1500168 (2015).

[15] I. Vaskivskyi, I. A. Mihailovic, S. Brazovskii, J. Gospodaric, T. Mertelj, D. Svetin, P. Sutar, and D. Mihailovic, Nat. Commun. **7**, 11442 (2016).

[16] L. Le Guyader, T. Chase, A. H. Reid, R. K. Li, D. Svetin, X. Shen, T. Vecchione, X. J. Wang, D. Mihailovic, and H. A. Durr, Struct. Dyn. **4**, 044020 (2017).

[17] T. Mertelj, P. Kusar, V. V. Kabanov, P. Giraldo-Gallo, I. R. Fisher, and D. Mihailovic, Phys. Rev. Lett. **110**, 156401 (2013).

[18] L. Stojchevska, M. Borovšak, P. Foury-Leylekian, J. P. Pouget, T. Mertelj, and D. Mihailovic, Phys. Rev. B **96**, 035429 (2017).

[19] S. Sugai, K. Murase, S. Uchida, and S. Tanaka, Physica B+C (Amsterdam) **105**, 405 (1981).

[20] K. R. A. Ziebeck, B. Dorner, W. G. Stirling, and R. Schollhorn, J. Phys. F **7**, 1139 (2001).

[21] S. Uchida and S. Sugai, Physica B+C (Amsterdam) **105**, 393 (1981).

[22] T. E. Stevens, J. Kuhl, and R. Merlin, Phys. Rev. B **65**, 144304 (2002).

[23] Y. Toda, F. Kawanokami, T. Kurosawa, M. Oda, I. Madan, T. Mertelj, V. V. Kabanov, and D. Mihailovic, Phys. Rev. B **90**, 094513 (2014).

[24] E. T. Heyen, S. N. Rashkeev, I. I. Mazin, O. K. Andersen, R. Liu, M. Cardona, and O. Jepsen, Phys. Rev. Lett. **65**, 3048 (1990).

[25] J. C. Petersen, S. Kaiser, N. Dean, A. Simoncig, H. Y. Liu, A. L. Cavalieri, C. Cacho, I. C. E. Turcu, E. Springate, and F. Frassetto, Phys. Rev. Lett. **107**, 177402 (2011).

[26] M. Eichberger, H. Schaefer, M. Krumova, M. Beyer, J. Demsar, H. Berger, G. Moriena, G. Sciaini, and R. J. D. Miller, Nature **468**, 799 (2010).

[27] K. Rossnagel, J. Phys.: Condens. Matter **23**, 213001 (2011).

[28] J. Wilson, F. DiSalvo, and S. Mahajan, Adv. Phys. **24**, 117 (1975).

[29] L. Perfetti, P. A. Loukakos, M. Lisowski, U. Bovensiepen, M. Wolf, H. Berger, S. Biermann, and A. Georges, New J. Phys. **10**, 053019 (2008).

[30] K. Haupt, M. Eichberger, N. Erasmus, A. Rohwer, J. Demsar, K. Rossnagel, and H. Schwoerer, Phys. Rev. Lett. **116**, 016402 (2016).

[31] W. L. McMillan, Phys. Rev. B **12**, 1187 (1975).

[32] R. Yusupov, T. Mertelj, V. V. Kabanov, S. Brazovskii, P. Kusar, J.-H. Chu, I. R. Fisher, and D. Mihailović, Nat. Phys. **6**, 681 (2010).